Journal of Artificial Organs (2019) 22:29–36
https://doi.org/10.1007/s10047-018-1072-z

ORIGINAL ARTICLE

Artificial Heart (Basic)

Shape optimization of a centrifugal blood pump by coupling CFD with metamodel-assisted genetic algorithm

Behnam Ghadimi[1] · Amir Nejat[1] · Seyed Ahmad Nourbakhsh[1] · Nasim Naderi[2]

Received: 12 May 2018 / Accepted: 29 September 2018 / Published online: 11 October 2018

Abstract

A centrifugal blood pump is a common type of pump used as a left ventricular assist device in the medical industries. Therefore, the improvement of the device bio-compatibility to reduce the blood damage and to increase the efficiency has become a major challenge. In the current work, a metamodel-assisted genetic algorithm is employed to simultaneously optimize the impeller and volute geometries of a typical centrifugal blood pump. The overall shape of the base design is inspired from HeartMate3 LVAD, and the main dimensions of the base design including inlet and outlet radius, blade angle distribution, volute cross-section area distribution, etc., are designed in our laboratory. Three different scenarios are investigated using three different objective functions, i.e., (1) hydraulic efficiency, (2) pressure head, and (3) hemolysis index (HI). The results showed that the shape optimized by pump efficiency has also nearly the same level of HI as the shape optimized by HI. Hence, to reduce computation time, one can use efficiency instead of HI as an objective function. However, one must check the HI level after such optimization to see whether it is within the acceptable range of HI for such bio application.

Keywords Hemolysis · Centrifugal blood pump · Optimization · Metamodel · Genetic algorithm

Introduction

The number of patients suffering from congestive heart failure (CHF), the final common destination of different forms of heart disease, grows annually, while only limited options are available to treat CHF. One of them is heart transplant that only around 2500 patients have this chance in the US in 2013 [1]. Continuous flow (CF) left ventricular assist devices (LVADs) are other options to treat CHF as a bridge to transplantation (BTT) or even as a destination therapy (DP). The CF LVADs operate at very high speeds, i.e., 4000–12,000 rpm [2], resulting in high shear stress regions. Increased shear stress represents one of the causes of hemolysis, platelet activation and acquired von Willebrand disease [3].

Until now, numerous amount of research on design and on hemolysis index comparison in different LVADs have been performed [4–6]. Nevertheless, there are few works on optimization of LVADs [7, 8]. One of the outstanding research on optimization of LVADs has been done by Zhu et al. [7] to optimize the diffuser blade of an axial blood pump. Unlike the axial LVADs, based on the authors' knowledge, there is no report on the optimization of centrifugal LVADs with specific bio-medical considerations. In addition, simultaneous optimization of the geometry of the impeller and the volute is not reported in the literature, which can be expressed as another novelty of this work. Furthermore, due to the large computation cost, the use of hemolysis index as an objective function has not been reported so far.

In the current work, an automated procedure is used to optimize the three-dimensional geometry of a centrifugal blood pump. To do this, three individual metamodels using artificial neural networks (ANNs) are trained to predict the pump pressure head, hemolysis index (HI), and pump hydraulic efficiency. Eleven geometrical parameters along

Electronic supplementary material The online version of this article (https://doi.org/10.1007/s10047-018-1072-z) contains supplementary material, which is available to authorized users.

✉ Amir Nejat
nejat@ut.ac.ir

[1] School of Mechanical Engineering, College of Engineering, University of Tehran, Tehran, Iran

[2] Rajaie Cardiovascular, Medical and Research Center, Tehran, Iran

with different constraints are used to create admissible geometrical shapes. The genetic algorithm (GA) is applied to optimize the pump geometry using the ANNs instead of the computationally much more expensive CFD solver. Three different scenarios are investigated using three different objective functions, i.e., (1) hydraulic efficiency, (2) pressure head, and (3) hemolysis index (HI).

Optimization method

The optimization algorithm including the geometry parameterization, sampling, CFD solver, ANN, and GA modules is presented in Fig. 1. The details of each step are discussed in the following sections.

Geometry parameterization

In this work, the overall shape of the base design is inspired from HeartMate3 LVAD, and the base geometry dimensions are designed in our laboratory using the methods which are described in [9]. Due to the human heart size, the variation of the pump inlet and outlet diameters is limited. Therefore, according to the LVADs in the markets the values of 18 mm, and 14 mm are considered for the pump inlet and outlet diameters, respectively [10].

The inlet radius, outlet radius and impeller height are selected as design parameters. Furthermore, the blade camber lines at the hub and shroud are defined by the distribution of the blade angle (β_u) in the radial direction. In the radial impellers of the centrifugal pumps the variation of the blade angle is almost linear [9]. Hence, the camber line circumferential position, θ, is defined as follows:

$$\beta_u = \beta_1(1-u) + \beta_2 u, \tag{1}$$

$$\mathrm{d}\theta = \frac{\tan\beta}{r}\mathrm{d}r, \tag{2}$$

where u is the non-dimensional radial length ($u \in [0, 1]$, 0 at the leading edge and 1 at the trailing edge), β_1 and β_2 are the blade angles at leading and trailing edges, respectively. These result in two design variables for the blade camber line definition.

The blade thickness distribution is assumed to be a function of four parameters: the leading edge thickness, t_{LE}, the thickness at 30% of the chord length, $t_{0.3}$, the trailing edge thickness, t_{TE}, and the leading edge ellipse ratio, $\mathrm{ER} = \frac{u_1}{t_{\mathrm{LE}}}$ (Fig. 2a). The trailing edge thickness is fixed at the value of 0.3 mm, due to construction constraints. This adds three other design variables to the optimization problem.

The contact surfaces between blades with impeller hub and shroud are filleted, and the radius of the fillet, R_f, is chosen as the ninth design parameter. To ensure the safe operation of all investigated pumps, the axial and radial gap sizes are borrowed from the well-known Heart-Mate 3 LVAD. Those gaps are fixed 0.5 mm radially and 1.0 mm axially [11].

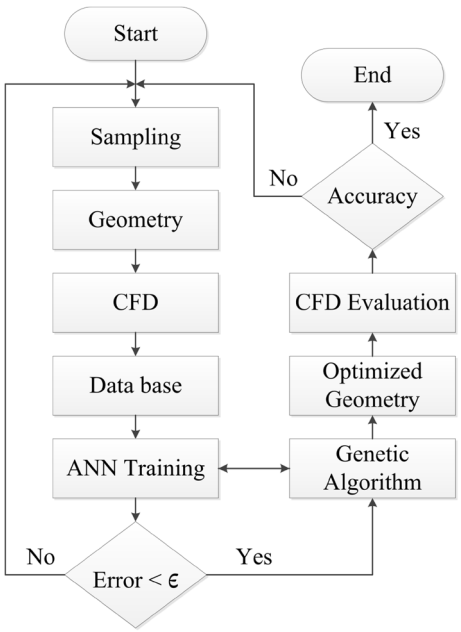

Fig. 1 Flowchart of optimization algorithm

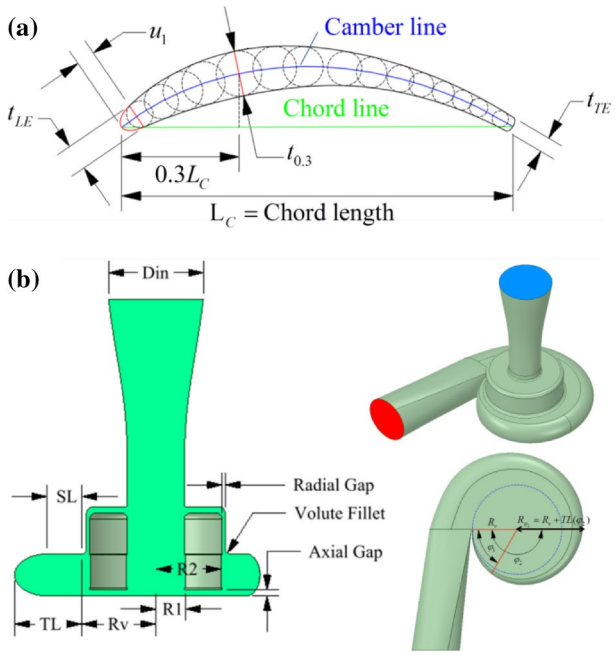

Fig. 2 **a** Parameters used to determine the blade thickness distribution, **b** The effective parameters in the design of volute geometry

In the centrifugal pumps, the cross-section area distribution of the volute is changed along the azimuthal angle to maintain a constant flow velocity and also to keep the pressure distribution as much uniform as possible. In the current work, the U-shaped volute is used (Fig. 2b). The volute height is obtained using impeller height and axial gap. Hence, the volute cross-section geometry is only a function of two parameters: the total radial length distribution, $R_\varphi = R_v + \mathrm{TL}(\varphi)$, and the fraction of volute straight length to total length, $F = \mathrm{SL}(\varphi)/\mathrm{TL}(\varphi)$, (Fig. 2b). To maintain a constant flow velocity in the azimuthal direction, the cross-section area of the volute should vary linearly with azimuthal angle. Hence, $\mathrm{TL}(\varphi)$ can be calculated using:

$$\mathrm{TL}(\varphi) = a\varphi \Rightarrow R_\varphi = R_v + a\varphi \tag{3}$$

where a is a constant number indicating the slope of area variation of the volute cross section. The blades number could also be a design parameter in the optimization procedure, but has been fixed to four (i.e., the number of blades in HeartMate 3) to reduce the computation cost. This leads to eleven design parameters. In addition to the above-mentioned descriptions, several other control points are used with only one degree of freedom by linking them to other parameters to guarantee the generation of realistic geometry.

Sampling

In computer experiments, a good experimental design covers the whole design space. Comprehensive reviews of different sampling methods have been carried out by Garud et al. [12]. They showed that the Sobol sequences have the best space filling ability with respect to Hammersley, Latin Hypercube Sampling (LHS), and Quasi-Monte Carlo sampling (QMCS), for a higher number of design variables. Accordingly, the Sobol sequences with eleven design variables are used to generate a sampling of the design space. The base design parameters and their ranges are shown in Table 1.

Table 1 The base design parameters and sampling range

	Design parameter	Dimension	Base design	Lower bound ($\mathbf{x}_L$)	Upper bound ($\mathbf{x}_U$)
1	R_1	mm	5	4	6
2	R_2	mm	11	10	12
3	h	mm	5.5	4.5	6.5
4	β_1	Degree	21	16	28
5	β_2	Degree	25	17	39
6	t_{LE}	mm	0.5	0.4	0.6
7	$t_{0.3}$	mm	1.2	0.9	1.5
8	ER	–	2	1	3
9	R_f	mm	0.5	0.4	0.6
10	a	–	1.5	1.2	1.8
11	F	–	0.5	0.2	0.8

Computational fluid dynamics

Hemolysis modeling

The most widely used correlation to calculate the HI is a power law function of [13]:

$$\mathrm{HI} = C t^\alpha \tau_s^\beta, \tag{4}$$

where t is the residence time, τ_s indicates the scalar shear stress, and C, α and β are empirical constants. In the current work, the reported power-law constants by Zhang et al. [13] are used ($C = 1.228 \times 10^{-5}$, $\alpha = 0.6606$, $\beta = 1.9918$).

In Eq. (4), the τ_s is calculated using the following equation [14]:

$$\tau_s = \left[\frac{1}{12}\sum\left(T_{ii} - T_{jj}\right)^2 + \frac{1}{2}\sum T_{ij}^2\right]^{1/2}$$
$$\text{where } T_{ij} = -P\delta_{ij} + \mu\left(\frac{\partial U_i}{\partial x_j} + \frac{\partial U_j}{\partial x_i}\right), \tag{5}$$

where T_{ij} is the stress tensor, P indicates the pressure, δ_{ij} is Kronecker delta ($\delta_{ij} = 1$ if $i = j$ and $\delta_{ij} = 0$ if $i \neq j$), U is the velocity, and μ is the fluid viscosity.

By defining $\mathrm{HI}' = \mathrm{HI}^{1/\alpha}$, a transport equation can be obtained by taking the total derivative of HI' with respect to time.

$$\frac{\mathrm{D}(\mathrm{HI}')}{\mathrm{D}t} = \left(C\tau_s^\beta\right)^{1/\alpha} \tag{6a}$$

$$\frac{\partial \mathrm{HI}'}{\partial t} + \mathbf{U}.\nabla \mathrm{HI}' = \left(C\tau_s^\beta\right)^{1/\alpha} \tag{6b}$$

where $\mathbf{U}$ is the velocity vector. CFD simulation of the flow inside the blood pump is obtained using ANSYS CFX 16.0 software, and the transport equation of the HI is introduced using the CEL Expression language in CFX. The SST $- k - \omega$ turbulence model is used for turbulence modeling. Due to the journal limitations in the number of words, the verification and validation of the numerical model are presented in the electronic supplementary material. The high-resolution scheme is used to discretize the advection terms in the momentum and HI scalar transport equations.

Blood properties

It is well known that blood is a non-Newtonian fluid, nevertheless, at high shear rates ($> 100\ s^{-1}$) it is treated as Newtonian fluid [4, 6]. Hence, in this work, a constant viscosity of 0.0035 kg/m.s and a density of 1050 kg/m^3 are used for the calculations.

Mesh and boundary conditions

The flow path of the centrifugal blood pump is meshed through a fully automated 3D unstructured mesh using a combination of tetrahedral and prism elements. The mesh independency is investigated, and the first layer height of the independent mesh is achieved 5e−06 [m], 1e−5 [m] at the blade rotary and stationary parts, respectively, with the total element number of 6.7 million for the base design.

As the boundary conditions, based on the physiological considerations the flow rate of 5 L/min is established at the pump inlet and the outlet pressure boundary condition is employed at the pump outlet. The impeller rotation speed of 5000 rpm is considered as rotating reference frame speed, and the stationary reference frame is used for other regions including inlet cannula, volute, and outlet cannula. At the interface of the rotary and stationary regions, the steady mixing-plane method is used. In this method, at the interface of rotating and stationary regions, the flow properties are circumferentially averaged. The HI value is calculated by integrating the mass-weighted HI values at the pump outlet, by supposing the zero HI value at the pump inlet.

$$\mathrm{HI}_{\mathrm{pump}} = \mathrm{HI}_{\mathrm{out}} - \mathrm{HI}_{\mathrm{in}} = \left(\frac{\int \mathrm{HI}\rho\mathbf{U}.\mathrm{d}A}{\int \rho\mathbf{U}.\mathrm{d}A} \right)_{\mathrm{out}} \tag{7}$$

In the above equation, ρ indicates the blood density, dA is the differential area at pump outlet plane and $\mathbf{U}$is the velocity vector. The mass-weighted averaging method is valid if the flow velocity distribution is almost uniform in the evaluation region. Accordingly, the pump outlet cannula is extruded 100 mm to have developed flow.

Artificial neural networks (ANNs)

ANNs have been shown to be effective tools for function approximation. In the current study, the feed-forward multilayer perceptron network with one input layer, two hidden layers, and one output layer has been used. The first input layer connects all eleven design variables to the network, whereas the last output layer produces the outputs (hydraulic efficiency, pressure head, and HI). The hyperbolic tangent function is performed as the activation function. The gradient descent algorithm is used to modify the weights of the networks according to the Widrow–Hoff delta rule [15].

Three individual set of metamodels are employed to predict the pump pressure head, hemolysis index (HI), and pump hydraulic efficiency to enhance the accuracy of each metamodel. To evaluate the accuracy of the trained ANNs, at each training procedure, 10% of data samples (0.1N) are randomly selected and removed from the training procedure. Then each remaining sample is considered as a test set and the rest $(0.9\mathrm{N}-1)$ of the samples are used as a training set. This is repeated 0.9N times, each time leaving out a different sample to use as the single test case. In the end, each metamodel consists of 0.9N ANNs, and the final output of the metamodel is the average of all 0.9N ANNs. When metamodel is created, the data that was removed from the training procedure is used to test the performance of the learned metamodel as new data. The obtained results for removed points error are described in "results" section.

Genetic algorithm (GA)

A genetic algorithm (GA) is employed to optimize a centrifugal LVAD pump by varying the geometric design parameters. GA uses evolution operations to generate new populations with higher average fitness values [16]. The following procedure is used:

1. A random initial population of potential solutions is generated;
2. The fitness value of each individual with the specified objective is evaluated using the three different metamodels as approximate models;
3. If the prescribed optimization criterion is not met, the genetic operations of selection, crossover, and mutation are applied to the population to create a new generation of potential solutions;
4. Step (2) and (3) are repeated until the optimization criterion is met.

Three different scenarios are carried out with the objective functions and constraints of:

$$\begin{aligned} &\text{minimize } \eta(\mathbf{x})^{-1} \\ &\text{subject to: } \begin{cases} \frac{H_b(\mathbf{x})-H(\mathbf{x})}{H_b(\mathbf{x})} \le 0.05 \\ \frac{\mathrm{HI}(\mathbf{x})-\mathrm{HI}_b(\mathbf{x})}{\mathrm{HI}_b(\mathbf{x})} \le 0.05 \end{cases} \\ &\mathbf{x} \in \left[\mathbf{x}_L, \mathbf{x}_U\right] \end{aligned} \tag{8}$$

$$\begin{aligned} &\text{minimize } H(\mathbf{x})^{-1} \\ &\text{subject to: } \begin{cases} \eta(\mathbf{x}) - \eta_b(\mathbf{x}) \geq 0.0 \\ \frac{\text{HI}(\mathbf{x}) - \text{HI}_b(\mathbf{x})}{\text{HI}_b(\mathbf{x})} \leq 0.05 \end{cases} \\ &\mathbf{x} \in \left[\mathbf{x}_L, \mathbf{x}_U\right] \end{aligned} \tag{9}$$

$$\begin{aligned} &\text{minimize } HI(\mathbf{x}) \\ &\text{subject to: } \begin{cases} \frac{H_b(\mathbf{x}) - H(\mathbf{x})}{H_b(\mathbf{x})} \leq 0.05 \\ \eta(\mathbf{x}) - \eta_b(\mathbf{x}) \geq 0.0 \end{cases} \\ &\mathbf{x} \in \left[\mathbf{x}_L, \mathbf{x}_U\right] \end{aligned} \tag{10}$$

where $\mathbf{x} = \left[x_1, x_2, \ldots, x_{11}\right]^T$ presents the design parameters. $\mathbf{x}_L$ and $\mathbf{x}_U$ are the lower and upper bound vectors which are expressed in Table 1, and the subscript b indicates the base design.

Results

To validate the metamodels, the errors of trained ANNs for removed points were calculated for different CFD sampling numbers. The results showed that increasing the CFD samples from 80 to 320 with the increment of 40 reduces the removed points error. However, increasing the sample number from 320 to 400 has little effect on the metamodel accuracy. Hence, in the current work, the 400 samples are used with the removed points error of 2.53%, 2.51%, and 1.63% for pressure head, HI, and hydraulic efficiency, respectively.

In Table 2, the results of the GA optimization for three different scenarios are presented. Furthermore, to investigate the effect of the metamodels error on optimization results, all the optimized geometries are simulated using CFD. The comparison of the pressure head, HI, and hydraulic efficiency obtained by the optimization procedure with the CFD results are included in this table showing good accuracy of the ANNs metamodels.

According to Table 2, in the first scenario, the relative enhancement in pump hydraulic efficiency is 12%, while this scenario allows both to decrease HI and to increase pressure head by the amounts of 6.21% and 11.3%, respectively.

In the second scenario, pump pressure head is increased 26.99% with respect to the base design, while the hemolysis index and the pump hydraulic efficiency are increased by the amounts of 7.34% and 5.8%, respectively. In this scenario, both increase in impeller height and the blade outlet angle lead to the higher tangential component of the absolute velocity at the blade outlet, resulting in a higher pressure head. Furthermore, increasing the tangential component of the absolute velocity leads to a lower absolute flow angle at the volute inlet. Hence, the volute cross-section area distribution is modified by lowering the coefficient a in Eq. 3 to properly gather the out-coming flow from the impeller.

In the third scenario, the HI value is decreased by 15.82%, while the pressure head is decreased by 5.31% and the pump hydraulic efficiency is relatively enhanced by the amount of 6.65%. In this scenario, the enhancement in the safe operation of the pump is mainly obtained by lowering the blade outlet angle and the impeller outlet radius. Although the optimization algorithm has endeavored to enhance the pressure head by increasing the blade height, decreasing both R_2 and β_2 has overcome the effect of blade height increasement, resulting in a lower pressure head with respect to the base design.

Table 2 The results of optimization procedure for three different scenarios

Parameter	Dimension	Base design	Scenario 1		Scenario 2		Scenario 3	
		CFD	Meta model	CFD	Meta model	CFD	Meta model	CFD
H	mmHg	93.39	102.77	103.99	119.32	118.60	89.25	88.52
$\text{HI}_{\text{out}} \times 10^4$	%	1.77	1.70	1.66	1.85	1.90	1.51	1.49
η	%	42.51	46.32	47.61	45.58	44.98	44.10	45.34
R_1	mm	5	4.10		4.18		4.90	
R_2	mm	11	10.97		11.29		10.55	
h	mm	5.5	5.77		6.29		6.08	
β_1	Degree	21	19.94		20.32		20.61	
β_2	Degree	25	23.48		29.44		25.34	
t_{LE}	mm	0.5	0.49		0.50		0.48	
$t_{0.3}$	mm	1.2	1.41		1.26		1.19	
ER	–	2	2.08		1.84		1.27	
R_{f}	mm	0.5	0.51		0.53		0.50	
a	–	1.5	1.33		1.26		1.26	
F	–	0.5	0.31		0.33		0.38	

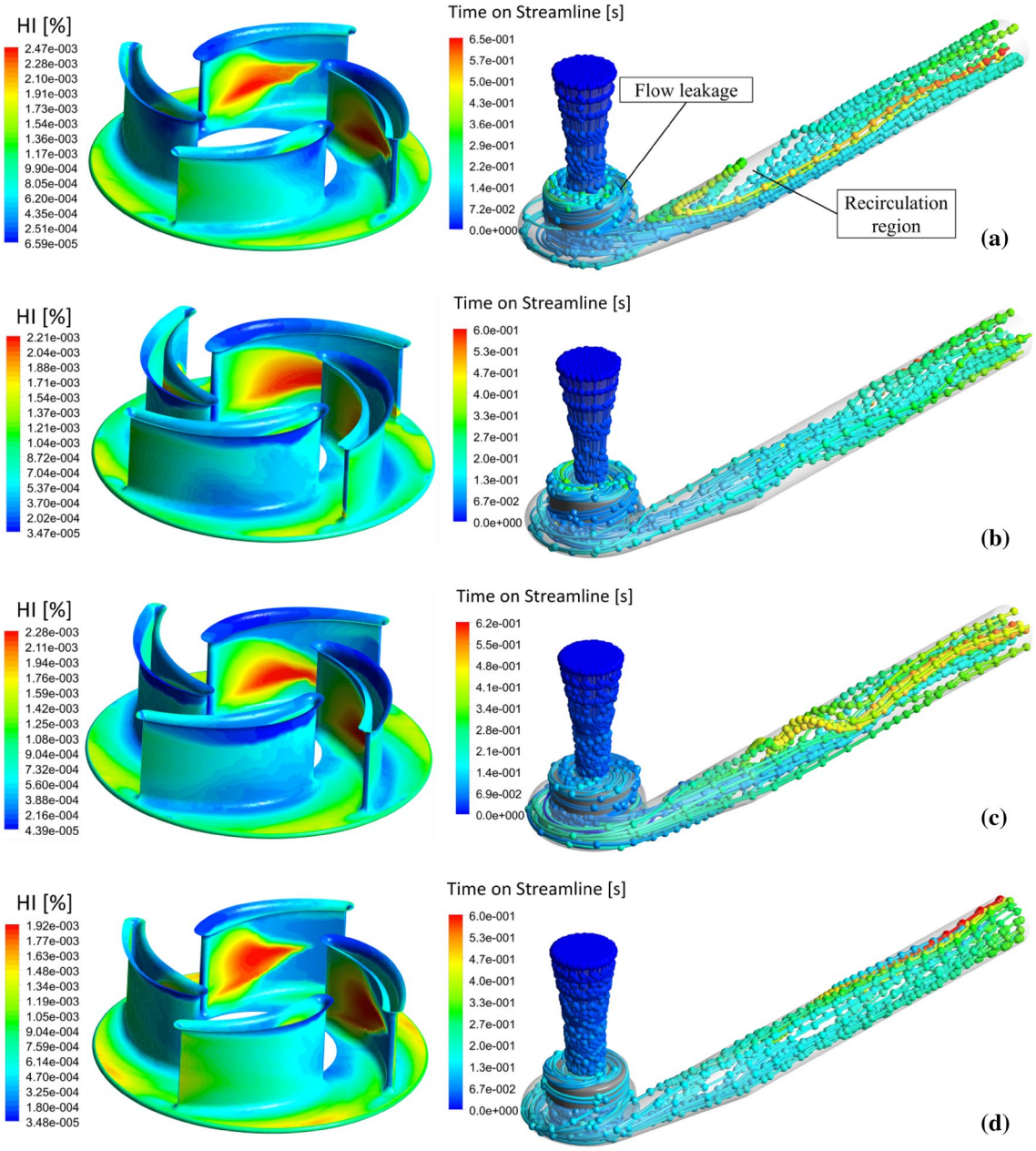

Fig. 3 (Left) Comparison of the hemolysis index distribution along the pump impeller, and (right) streamlines tracking the fluid residence time (the time interval between two successive balls is 0.01 s) for **a** base design, **b** scenario 1, **c** scenario 2, and **d** scenario 3

In Fig. 3, the HI distribution at the blade surface and the streamlines tracking fluid residence times in the three optimized geometries are compared to the base design. The initial time at the inlet of the pump is considered equal to zero. Since the velocity in the blade suction side is higher than the blade pressure side, the shear stress and consequently HI value at the blade suction side is higher than the blade pressure side. In the third scenario, the impeller has the minimum length ($R_2 - R_1$) with respect to the other three presented geometries leading to a lower blood contact area with pump impeller and lower flow residence time at high shear stress region, thus reducing the hemolysis index.

Some blood is recirculated at the gap between the rotating impeller and the stationary casing (volute). The recirculation flow is damped at the pump discharge pipe. In the third scenario, the blood recirculation from impeller outlet to impeller inlet through the pump gap is lower than the others, because of the lower pressure gradient between impeller inlet and outlet with respect to the other cases. In the base design, a recirculation zone at the entry of the pump

Table 3 The results of the optimized geometries at the same operating conditions

Parameter	Dimension	Base Design	Scenario1	Scenario 2	Scenario 3
H	mmHg	93.39	93.93	93.46	93.20
Q	Lit/min	5.0	5.0	5.0	5.0
n	rpm	5000	4775	4510	5110
$HI_{out} \times 10^4$	%	1.77	1.56	1.68	1.51
η	%	42.51	47.22	44.35	45.69

discharge pipe is declared; while in the first and the third scenarios the streamlines declare almost uniform flow at the pump discharge pipe. Furthermore, owing to the higher pressure head in the second scenario and correspondingly higher pressure gradient, in this scenario the small helical circulation flow is observed.

To determine the best scenario, all the obtained geometries must be evaluated under the same operating conditions. Hence, a trial and error procedure was implemented to find the operating speed of the optimized geometries in which the head and mass flow rate of the base design is produced. The results are presented in Table 3. According to this table, the first and second scenarios are able to produce the same flow rate and pressure head as base design in lower impeller rotational speed. However, the impeller speed in the third scenario is a bit higher than the base design, owing to its lower impeller size.

At the same operating conditions, the maximum enhancement in pump hydraulic efficiency is achieved in the first scenario and also the reduction of hemolysis index in this scenario is just slightly less than the third scenario, in which the optimization goal is hemolysis index minimization.

Discussion

The shape optimization of the blood pump is a challenging problem due to the high simulation cost and the complex nature of hemolysis. In the current work, the number of grids for the base design was 6.7 million requiring almost 15 h to run in desktop computers with the processor of Intel® Core™ i7 4770K, 3.5 GHz and installed RAM of 32 GB. Hence, for an eleven-variable optimization problem using GA, assuming 110 number of populations (10 population for each variable), and 40 iterations for GA convergence, the total computation time would be 7.5 years for each scenario. In the current work, the ANNs metamodels were trained by only 400 CFD results which take 9 months to run on one computer. However, using metamodels enabled us to perform the simulations on three different computers which reduced the computation costs to three months.

The results showed that the blade inlet and outlet angle play a significant role in pump efficiency and HI. Hence, one can reduce the blade outlet angle to increase the pump efficiency and decrease the HI. Meanwhile, increasing the blade height will increase the pump efficiency by reducing the inlet velocity. However, it should be noted that decreasing the velocity at the impeller inlet requires some modifications on blade inlet angle.

It is worth mentioning that the HI calculation needs finer grid than efficiency calculation. Furthermore, we need to solve an extra transport equation to calculate HI. As a result, the computation cost for the HI objective is roughly 3 times more than the computation cost for efficiency objective. In addition, the results of the current work showed that the shape optimized by pump efficiency as an objective function results in almost the same level of HI and higher improvement in efficiency compared with the case that the shape optimized by HI as the objective function. Hence, to save time, one can use efficiency as an objective function instead of HI. However, one must check the HI level after such optimization to see whether it is within the acceptable range of HI for such bio application. In other words, the HI must be considered in any advanced optimization procedures in bio-pumps, either as an objective function or as a final check.

Conclusion

In this study, a fully automated optimization procedure was developed and successfully employed for the optimization of a centrifugal blood pump. Three different optimization scenarios were carried out, by considering the efficiency, pressure head and hemolysis index as optimization goals in scenario 1–3, respectively. At the same operating conditions, the results showed that the hydraulic efficiency was improved 11.1%, 4.3%, and 6.1% in scenario 1–3, respectively, while the HI was reduced 11.8%, 5.1%, and 14.7% in those scenarios. In blood pumps, the HI parameter is more important than the pump efficiency. Hence, the third scenario, in which the HI has the lowest value, presents a more reliable geometry than the other scenarios. Nevertheless, the first scenario gives a considerable improvement in pump hydraulic efficiency with nearly the same level of HI reduction with respect to the third scenario. Therefore, due to the higher computation cost of HI, one can use the first scenario to optimize the blood pumps. However, it should be noted that the pump optimized by the first scenario is only a good design candidate for the pump with lower HI, and it is not always the pump with the lowest HI.

Acknowledgements This research is sponsored by the Iran National Science Foundation (INSF) with the Project No. of 95837323.

Compliance with ethical standards

Conflict of interest The authors declared that there are no conflicts of interest.

References

1. Mozaffarian D, Benjamin EJ, Go AS, Arnett DK, Blaha MJ, Cushman M, et al. Heart disease stroke statistics—2015 update. Circulation. 2015;131:e29–322.
2. Fraser KH, Taskin ME, Griffith BP, Wu ZJ. The use of computational fluid dynamics in the development of ventricular assist devices. Med Eng Phys. 2011;33:263–80.
3. Bartoli CR, Kang J, Zhang D, Howard J, Acker M, Atluri P, et al. Left ventricular assist device design reduces von Willebrand factor degradation: a comparative study between the HeartMate II and the EVAHEART left ventricular assist system. Ann Thorac Surg. 2017;103:1239–44.
4. Fraser KH, Zhang T, Taskin ME, Griffith BP, Wu ZJ. A quantitative comparison of mechanical blood damage parameters in rotary ventricular assist devices: shear stress, exposure time and hemolysis index. J Biomech Eng. 2012;134:81002.
5. Hosoda K, Ishii K, Isoyama T, Saito I, Inoue Y, Ariyoshi K, et al. Computational fluid dynamics analysis of the pump parameters in the helical flow pump. J Artif Organs. 2014;17:9–15.
6. Khan TI, Sheh Zad H, Lazoglu I, Yalcin O. Development of a novel shrouded impeller pediatric blood pump. J Artif Organs. 2018;21:142–9.
7. Zhu L, Zhang X, Yao Z. Shape optimization of the diffuser blade of an axial blood pump by computational fluid dynamics. Artif Organs. 2010;34:185–92.
8. Yu H, Janiga G, Thévenin D. Computational fluid dynamics-based design optimization method for archimedes screw blood pumps. Artif Organs. 2016;40:341–52.
9. Nourbakhsh SA, Jaumotte BA, Hirsch C, Parizi HB, editors. Turbopumps and Pumping Systems. Berlin: Springer; 2007.
10. Bourque K, Cotter C, Dague C, Harjes D, Dur O, Duhamel J, et al. Design rationale and preclinical evaluation of the HeartMate 3 left ventricular assist system for hemocompatibility. ASAIO J. 2016;62:375–83.
11. Kyo S, editor. Ventricular assist devices in advanced-stage heart failure. Tokyo: Springer; 2014.
12. Garud SS, Karimi IA, Kraft M. Design of computer experiments: a review. Comput Chem Eng. 2017;106:71–95.
13. Zhang T, Taskin ME, Fang H-B, Pampori A, Jarvik R, Griffith BP, et al. Study of flow-induced hemolysis using novel Couette-type blood-shearing devices. Artif Organs. 2011;35:1180–6.
14. Faghih MM, Keith Sharp M. Extending the power-law hemolysis model to complex flows. J Biomech Eng. 2016;138:124504.
15. Haykin S. Neural networks: a comprehensive foundation. 2nd ed. London: Pearson Education Inc.; 1999.
16. Koza JR. Genetic programming: on the programming of computers by means of natural selection. Cambridge: Massachusetts Institute of Technology Press; 1992.